arXiv:1212.0648v1 [hep-ph] 4 Dec 2012

$X(3872)$ is not a true molecule

Susana Coito* and George Rupp†
Centro de Física das Interacções Fundamentais, Instituto Superior Técnico,
Technical University of Lisbon, P-1049-001 Lisboa, Portugal

Eef van Beveren‡
Centro de Física Computacional, Departamento de Física,
Universidade de Coimbra, P-3004-516 Coimbra, Portugal

(Dated: December 5, 2012)

The wave function of the charmonium-like meson $X(3872)$ is expected to have a very significant $D^0\overline{D}^{*0}$ component, as the latter threshold lies only 0.16 MeV above the meson's mass. Some conclude from this mass coincidence that $X(3872)$ is a meson-meson molecule, whatever the dynamics giving rise to the state. This would imply that the $D^0\overline{D}^{*0}$ component of the $X(3872)$ wave function is the only relevant one. In the present paper we study this issue by employing a soluble model for a $^3P_1$ $c\bar{c}$ state coupled to an S-wave $D^0\overline{D}^{*0}$ decay channel, communicating via the $^3P_0$ mechanism. The model is a simplified, coordinate-space version of the resonance-spectrum expansion previously employed in a detailed investigation of $X(3872)$'s nature. The resulting two-component wave function is calculated for different values of the binding energy (BE) and the transition radius a. Thus, a significant $c\bar{c}$ component is found in all situations. However, the long tail of the $D^0\overline{D}^{*0}$ wave function, in the case of small BEs, strongly limits the $c\bar{c}$ probability, which roughly lies in the range 7–11%, for the true BE of 0.16 MeV and a between 2 and 3 GeV^{-1}. Furthermore, a reasonable value of 7.8 fm is obtained for the $X(3872)$ r.m.s. radius at the physical mass, as well as an S-wave $D^0\overline{D}^{*0}$ scattering length of 11.6 fm. Finally, the $\mathcal{S}$-matrix pole trajectories as a function of coupling constant show that $X(3872)$ can be generated either as a dynamical pole or as one connected to the bare $c\bar{c}$ confinement spectrum, depending on details of the model. From these results we conclude that $X(3872)$ is not a genuine meson-meson molecule, nor actually any other mesonic system with non-exotic quantum numbers, due to the inevitable mixing with the corresponding quark-antiquark states.

PACS numbers: 14.40.Pq, 14.40.Lb, 12.39.Pn, 11.55.Ds

I. INTRODUCTION

The Belle Collaboration discovered [1] the charmonium-like state $X(3872)$ almost a decade ago, observing it the decay $B^\pm \to K^\pm\pi^+\pi^- J/\psi$, with a significance in excess of 10σ. The new meson was then confirmed by CDF [2], D0 [3], BABAR [4], and recently also by LHCb [5]. In the 2012 PDG tables [6], $X(3872)$ is listed with a mass of 3871.68 ± 0.17 MeV and a width $\Gamma < 1.2$ MeV. As for the quantum numbers, the possibilities are $J^{PC} = 1^{++}$ and $J^{PC} = 2^{-+}$ according to the PDG [6]. The positive C-parity assignment resulted out from an analysis of angular distributions by CDF [7]. Recently, observation of the decay to $\gamma J/\psi$ by Belle [8] unambiguosly confirmed $C = +$. For further experiments on $X(3872)$ production, see Ref. [6].

On the theory side, the discussion about the nature of $X(3872)$ continues most vivid. Although the PDG [6] lists 1^{++} and 2^{-+} as the meson's possible quantum numbers, and a recent BABAR analysis [9] of the 3π invariant mass distribution in the decay $X(3872) \to \omega J/\psi$ even seems to slightly favor the 2^{-+} assignment, most model builders describe the state as an axial vector. For instance, model calculations of semi-inclusive $B \to \eta_{c2} + X$ processes [10] as well as electromagnetic η_{c2} decays [11] have been shown to disfavor the 2^{-+} scenario. The same conclusion was reached in a tetraquark description of $X(3872)$ [12], while pion exchange in a molecular picture would be repulsive in this case [13] and so inhibitive of a bound state. Finally, unquenching a $1\,^1D_2$ $c\bar{c}$ state by including meson-meson loops can only further lower the bare mass, which lies in the range 3.79–3.84 GeV for all quenched quark models we know of, thus making a 2^{-+} charmonium resonance at 3.872 GeV very unlikely [14]. For further information and more references concerning $X(3872)$, see e.g. a recent review [15], as well as our prior coupled-channel analysis [14].

The first suggestion of possible meson-meson molecules bound by pion exchange, in particular a DD^{*}[1] state with quantum numbers 1^{++} or 0^{-+}, was due to Törnqvist [13]. With the discovery of $X(3872)$ just below the D^0D^{*0} threshold, this idea was revived, of course. In the present

---

*Electronic address: susana.coito@ist.utl.pt
†Electronic address: george@ist.utl.pt
‡Electronic address: eef@teor.fis.uc.pt

[1] Henceforth, we omit the bar in $D\overline{D}^*$, for notational simplicity.

paper, we intend to study the issue, not from Törnqvist's pion-exchange point of view, but rather as regards its possible implications for models based on quark degrees of freedom. In this context, it is worthwhile to quote from Ref. [16], in which a molecular interpretation is advocated (also see Ref. [17]):

> *"Independent of the original mechanism for the resonance, the strong coupling transforms the resonance into a bound state just below the two-particle threshold if $a > 0$ or into a virtual state just above the two-particle threshold if $a < 0$. If $a > 0$, the bound state has a molecular structure, with the particles having a large mean separation of order a."*

(Note that, here, a is the S-wave scattering length.) Also:

> *"In this case* [1^{++}]*, the measured mass M_X implies unambiguously that X must be either a charm meson molecule or a virtual state of charm mesons."*

In face of these peremptory claims about the molecular picture, we believe it is of utmost importance to study in detail the $X(3872)$ wave function for a model in which the *mechanism* generating the meson is quark confinement combined with strong decay. Thus, we employ a simplified, coordinate-space version of the coupled-channel model used recently [14] to describe $X(3872)$ as a unitarized and mass-shifted $2\,^3P_1$ charmonium state. The model's exact solvability then allows to obtain analytic expressions for the wave-function components, and follow bound-state as well as resonance poles in different Riemann sheets.

The model is outlined in Sec. II, with details moved to Appendices A and B. Section III is devoted to $\mathcal{S}$-matrix pole trajectories as a function of the two free parameters. In Sec. IV the two-component wave function is analyzed for several parameter sets, and is then used in Sec. V to compute $c\bar{c}$ probabilities and root-mean-square (r.m.s.) radii. The dynamical vs. confinement nature of the poles is discussed in Sec. VI. Conclusions are drawn in Sec. VII.

II. THE COUPLED $c\bar{c}$-D^0D^{*0} SYSTEM

In our previous work on $X(3872)$ [14], we described the state as a unitarized radially excited 1^{++} charmonium resonance, by employing the resonance-spectrum-expansion (RSE) [18] formalism. The RSE description of $X(3872)$ amounted to coupling the most relevant meson-meson channels allowed by the Okubo-Zweig-Izuka (OZI) rule to a spectrum of bare 1^{++} $c\bar{c}$ states, and also the OZI-suppressed but experimentally observed [6] $\rho^0 J/\psi$ and $\omega J/\psi$ channels. Thus, we found that unquenching shifts the bare $2\,^3P_1$ state more than 100 MeV downwards, which settles as a very narrow resonance slightly below or on top of the D^0D^{*0} threshold. However, the RSE approach does not allow to obtain wave functions in a straightforward fashion. So for the purpose of the present paper, we resort to the equivalent [19] coordinate-space coupled-channel formalism of Ref. [20], which was used to study the influence of strong decay channels on hadronic spectra and wave functions, besides several more specific phenomenological applications. Furthermore, since here we do not aim to describe all aspects of the $X(3872)$ resonance in a detailed way, but rather want to focus on the importance of the charmonium component in the wave function, we restrict ourselves henceforth to a simple two-channel system, viz. a $^3P_1$ $c\bar{c}$ state coupled to an S-wave D^0D^{*0} channel, the latter being the dominant one, observed in the $D^0\overline{D}^0\pi^0$ mode [6]. A partial study of this problem was already carried out in Ref. [21].

Consider now a system composed of a confined $q\bar{q}$ channel coupled to a meson-meson channel M_1M_2. Confinement is described through a harmonic-oscillator (HO) potential with constant frequency ω, having spectrum

$$E = (2\nu + l_c + \frac{3}{2})\,\omega + m_q + m_{\bar{q}} \; , \tag{1}$$

where ν is the radial quantum number, l_c the $q\bar{q}$ orbital angular momentum, and $m_q = m_{\bar{q}} = 2\mu_q$ the constituent quark mass. In the scattering channel, no direct interactions between the two mesons are considered, with μ_f and l_f being the reduced two-meson mass and orbital angular momenta in the free channel, respectively. Transitions between the two channels are modeled via an off-diagonal delta-shell potential with strength g, which mimics string breaking at a well-defined distance a. The corresponding Hamiltonian, transition potential, and 2×2 matrix Schrödinger equation are given in Eqs. (2)–(5), with the usual definition $u(r) = rR(r)$, where $R(r)$ is the radial wave function. The exact solution to these equations is derived in Appendix A:

$$h_c = \frac{1}{2\mu_c}\left(-\frac{d^2}{dr^2} + \frac{l_c(l_c+1)}{r^2}\right) + \frac{\mu_c\omega^2r^2}{2} + m_q + m_{\bar{q}} \; , \tag{2}$$

$$h_f = \frac{1}{2\mu_f}\left(-\frac{d^2}{dr^2} + \frac{l_f(l_f+1)}{r^2}\right) + m_{M_1} + m_{M_2} \; , \tag{3}$$

$$V = \frac{g}{2\mu_c a}\delta(r-a) \; , \tag{4}$$

$$\begin{pmatrix} h_c & V \\ V & h_f \end{pmatrix}\begin{pmatrix} u_c \\ u_f \end{pmatrix} = E\begin{pmatrix} u_c \\ u_f \end{pmatrix} \; . \tag{5}$$

Once the 1×1 $\mathcal{S}$ matrix (cf. Eq. (A13)) has been constructed from the wave function, possible bound or virtual states as well as resonances can be searched for. These occur at real or complex energies for which $\mathcal{S}$ blows up, or equivalently, when $\cot\delta_{l_f}(E) = i$ (cf. Eq. (A12)). Thus, unlike the pure HO spectrum, which is a real and discrete set of energies, the "unquenched" spectrum given by Eq. 5 includes complex energies, too, some of which even have no obvious connection to the original, "bare" levels. The corresponding poles, called *dynamical*, are the result of attraction in the meson-meson channel generated by the interaction with intermediate quark-antiquark states. The light scalar mesons $f_0(500)$, $K_0^*(800)$, $f_0(980)$, and $a_0(980)$ [6] are archetypes of such resonances [22]. On the other hand, we designate by *confinement poles* the ones that can be linked straightforwardly to the bare states. Nevertheless, we shall show below — as we already demonstrated in previous work — that these two types of resonances are not so distinct after all, since minor parameter changes may transform one kind into the other. But regardless of the type of pole, the corresponding radial quantum number in Eq. (6) is related to the energy of the coupled-channel system by

$$\nu(E) = \frac{E - 2m_c}{2\omega} - \frac{l_c + 3/2}{2}. \tag{6}$$

Only in the uncoupled case, that is, for $g = 0$, one recovers the original HO spectrum, with $\nu = 0, 1, 2, \ldots$.

Now we apply the formalism to the coupled $c\bar{c}$-D^0D^{*0} system. The $c\bar{c}$ channel is assumed to be in a $^3P_1$ state, i.e., with $l_c = 1$, implying the D^0D^{*0} channel to have $l_f = 0$ or 2. Nevertheless, we shall restrict ourselves here to the S-wave channel only, which will be strongly dominant, especially near threshold. The fixed parameters are given in Table I, where the meson masses are from the PDG [6], while the HO frequency ω and the constituent charm quark mass m_c are as originally determined in Ref. [23] and left unaltered ever since. Thus, from Eq. (1) we get the lowest two HO states at $E_0 = 3599$ MeV and $E_1 = 3979$ MeV, respectively. The former should give rise — after unquenching — to the $1\,^3P_1$ charmonium state $\chi_{c1}(1P)$ [6], with mass 3511 MeV, while the latter is the bare $2\,^3P_1$ state, which cannot so easily be linked to resonances in the PDG tables, though both $X(3940)$ and $X(3872)$ are possible candidates, in view of their mass and dominant DD^* decay mode [6]. However, $X(3940)$ may just as well be the, so far unconfirmed, $2\,^1P_1$ (1^{+-}) state $h_c(2P)$ [14].

The two remaining parameters, viz. the string-breaking distance a and the global coupling g, have to be adjusted to the experimental data. Nevertheless, these parameters are not completely free, as they both have a clear physical interpretation, albeit of an empirical nature. Thus, a is the average interquark separation at which $^3P_1$ quark-pair creation/annihilation is supposed to take place, while g is the overall coupling strength for such processes. Note that we do not assume a particular microscopic model for string breaking inspired by QCD, like e.g. in a very recent paper [24]. Still, the values of a found in the present work are in rough agreement with our prior model findings, and even compatible [25] with a lattice study of string breaking in QCD [26]. Concretely, we have been obtaining values of a in the range 1–4 GeV^{-1} (0.2–0.8 fm), logically dependent on quark flavor, since the string-breaking distance will scale with the meson's size, being smallest for bottomonium. As for the coupling parameter g, its empirical value will depend on a, but also on the set of included decay channels. In realistic calculations, values of the order of 3 have been obtained (see e.g. our previous paper [14] on the $X(3872)$).

TABLE I: Fixed parameters.

Parameter	ω	m_c	m_{D^0}	$m_{D^{*0}}$	$m_{D^0} + m_{D^{*0}}$
Value (MeV)	190	1562	1864.86	2006.98	**3871.84**

III. POLES

The crucial test the present model must pass is its capability of generating a pole near the D^0D^{*0} threshold. Indeed, a dynamical pole is found slightly below threshold for different combinations of the free parameters a and g, several of which are listed in Table II. Examples are here given of bound states, virtual bound states, and below-threshold resonances, the latter ones only occurring for S-wave thresholds as in our case. Note that poles of both virtual bound states and resonances lie on the second Riemann sheet, i.e., the relative momentum has a negative imaginary part. From this table we also observe that larger and larger couplings are needed to generate a pole close to threshold when a approaches the value 3.5 GeV^{-1}. We shall see below that this is due to the nodal structure of the bound-state wave function.

Although a dynamical pole shows up near the D^0D^{*0} threshold, there still should be a confinement pole connected to the first radial $^3P_1$ excitation at 3979 MeV. Well, we do find such a pole, for each entry in Table II. In Table III a few cases are collected, with the parameters tuned to generate a dynamical pole at precisely the

TABLE II: Bound states (BS), virtual bound states (VBS), and resonances closest to threshold, for various g and a combinations.

a (GeV^{-1})	g	Pole (MeV)	Type
2.0	1.149	3871.84	VBS
2.5	1.371	3871.84	VBS
3.0	2.142	3871.84	VBS
3.1	2.503	3871.84	VBS
3.2	2.531	$3871.84 - i12.01$	resonance
3.3	3.723	$3871.84 - i\ 4.45$	resonance
3.4	7.975	$3871.84 - i\ 0.39$	resonance
3.5	∞		-
2.0	1.152	3871.84	BS
2.5	1.373	3871.84	BS
3.0	2.145	3871.84	BS
3.1	2.507	3871.84	BS
3.2	3.083	3871.84	BS
3.3	4.194	3871.84	BS
3.4	8.254	3871.84	BS
3.5	∞		-

TABLE III: Pole doubling: pairs of poles (in MeV) for some sets of a and g values, chosen such that the dynamical pole settles at the $X(3872)$ PDG [6] mass.

a (GeV^{-1})	g	Dynamical Pole	Confinement Pole
2.0	1.172	3871.68	$4030.50 - i136.51$
2.5	1.403	3871.68	$4063.27 - i124.07$
3.0	2.204	3871.68	$4101.48 - i\ 88.03$
3.4	8.623	3871.68	$4185.85 - i\ 20.63$

$X(3872)$ PDG [6] mass of 3871.68 MeV. Note, however, that the associated confinement pole is not necessarily of physical relevance, since at the corresponding energy several other strong decay channels are open, which no doubt will have a very considerable influence and possibly even change the nature of both poles. As a matter of fact, in our prior paper [14], with all relevant two-meson channels included, the $X(3872)$ resonance was found as a confinement pole, whereas dynamical poles were only encountered very deep in the complex energy plane, without any observable effect at real energies. So here we show these results only to illustrate that pole doubling may occur when strongly coupling S-wave thresholds are involved, as we have observed in the past in the case of e.g. the light scalar mesons [22] and the $D^*_{s0}(2317)$ [27]. The issue of confinement vs. dynamical poles will be further studied in Sec. VI.

In order to better understand the dynamics of the different poles, we plot in Fig. 1 pole trajectories in the complex energy plane as a function of the coupling constant g, and for three diferent values of a. For vanishing g, the dynamical pole acquires a negative infinite imaginary part and so disappears in the continuum, whereas the confinement pole moves to the real energy level of the bare $2\,^3P_1$ state, i.e., 3979 MeV. As g increases, and for both $a = 2.0$ GeV^{-1} and $a = 3.0$ GeV^{-1}, the dynamical pole moves to the real axis below threshold, becoming first a virtual bound state and then a genuine bound state. Note that, in the latter case, the real part twice attains the $X(3872)$ mass even before the pole reaches the real axis, but the corresponding imaginary parts are much too large as compared with experiment [6], so only the bound state can be considered physical. Finally, for $a = 3.5$ GeV^{-1} the pole does never reach the real axis, which would require an infinite coupling. For the other parameter sets listed in Table II, we find intermediate situations. Another feature we can observe for all trajectories is an initial attraction and subsequent repulsion between the dynamical and the confinement poles.

IV. WAVE FUNCTION

Now we are in a position to study the $X(3872)$ bound-state wave function in several situations. We choose two values for the string-breaking parameter, viz. $a = 2.0$ GeV^{-1} and $a = 3.0$ GeV^{-1}. In Table IV five different binding energies (BEs) are chosen with respect to the D^0D^{*0} channel, including the PDG [6] value labeled by X. We have computed and normalized (see Appendix A) the two-component radial wave function $R(r)$ was computed and normalized for each of the five cases. In Fig. 2 we depict the cases labeled by A, X and D, the other two representing intermediate situations. A general feature we immediately observe is the typical S-wave behavior of the D^0D^{*0} wave-function component R_f, while the $c\bar{c}$

FIG. 1: Pole trajectories of dynamical (left) and confinement (right) poles as a function of g, for a=2.0 GeV^{-1} (top), 3.0 GeV^{-1} (middle), and 3.5 GeV^{-1} (bottom), respectively. In the last case, there is no bound state near threshold. Note: (i) poles in Table. III are here marked by $*$; (ii) arrows along curves indicate increasing $\boldsymbol{g}$.

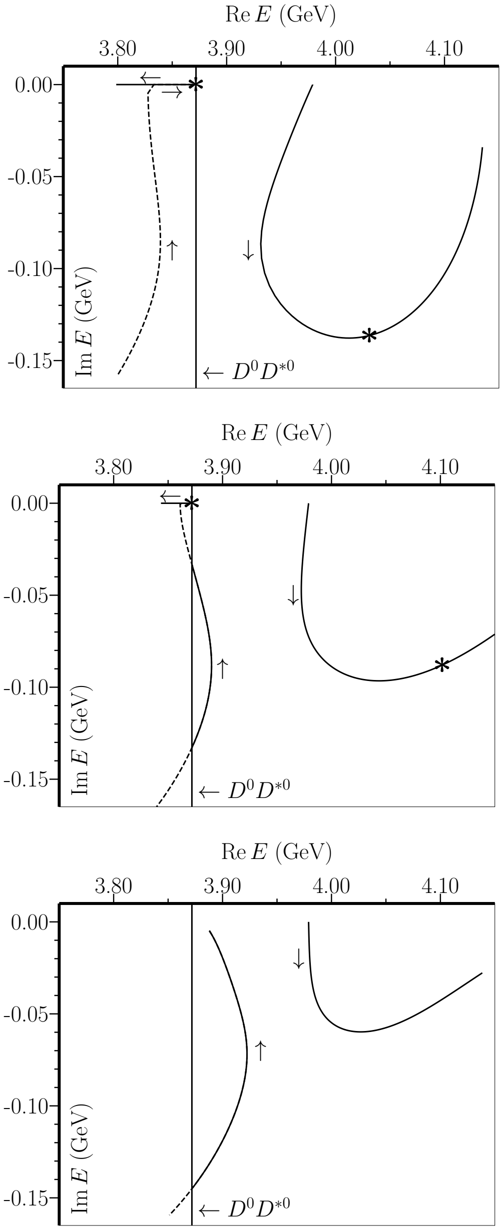

TABLE IV: Five chosen binding energies (BEs) in the D^0D^{*0} channel, for two different a values and the corresponding couplings g.

a (GeV^{-1})		2.0		3.0	
Label	BE (MeV)	g	Pole	g	Pole
A	0.00	1.152	3871.84	2.145	3871.84
B	0.10	1.167	3871.74	2.191	3871.74
X	**0.16**	**1.172**	**3871.68**	**2.204**	**3871.68**
C	1.00	1.207	3870.84	2.311	3870.83
D	10.00	1.373	3861.82	2.899	3861.84

wave function R_c is a P state, having one node. Also, $|R_f|$ is larger than $|R_c|$ in most situations, for all r, except for unphysically large BEs (cf. plot D). Nevertheless, the two components are of comparable size for intermediate r values. Then, as the BE becomes smaller, the tail of R_f grows longer, as expected, whereas R_c always becomes negligible for distances larger than roughly 11–12 GeV^{-1}. Now, the increased R_f tail affects the normalization of *both* R_c and R_f. Thus, the ratio $|R_f(r)|/|R_c(r)|$ is quite robust for most r values, as it does not significantly change with the BE.

FIG. 2: Normalized two-component radial wave function $R(r)$ for three BEs, corresponding to labels A, X, D in Table IV, and two a values. Upper curves: $R_f(r)$; lower curves: $R_c(r)$. Left: $a = 2$ GeV^{-1}; right: $a = 3$ GeV^{-1}.

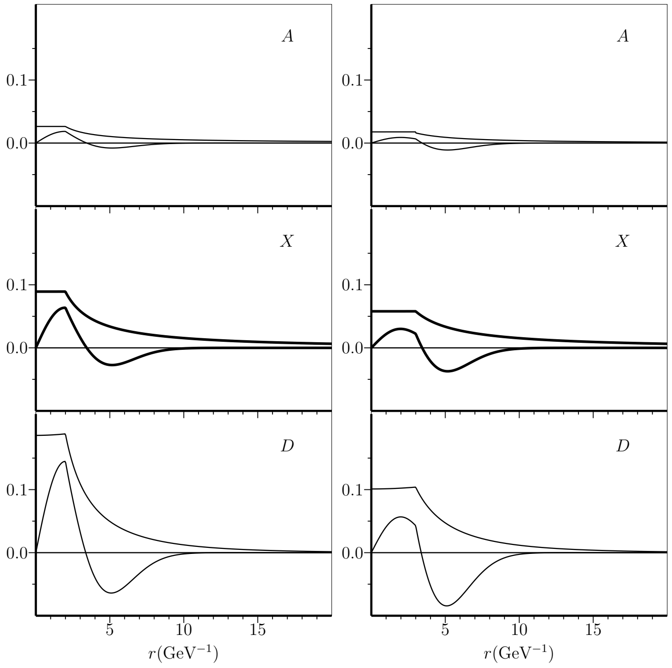

V. PROBABILITIES AND R.M.S. RADII

TABLE V: Probabilities (in %) of the two wave-function componenents, for the cases specified in Table IV.

a (GeV^{-1})	channel	A	B	**X**	C	D
2.0	$c\bar{c}$	0.63	6.00	**7.48**	16.98	39.68
2.0	D^0D^{*0}	99.37	94.00	92.52	83.02	60.32
3.0	$c\bar{c}$	0.97	9.01	**11.18**	24.65	55.54
3.0	D^0D^{*0}	99.03	90.99	88.82	75.35	44.46

Having derived the $X(3872)$ wave function for several scenarios, we can now straightforwardly compute the relative probabilities of the $c\bar{c}$ and D^0D^{*0} components (see Appendix A), with the results given in Table V, for the five BEs and two a values from Table IV. Note that the probability in the D^0D^{*0} channel is only computed for normalization purposes, since in a more realistic calculation at least the $D^{\pm}D^{*\mp}$ component would acquire a non-negligible probability as well, as the corresponding threshold lies only 8 MeV higher. Nevertheless, our simplification is unlikely to have an appreciable effect on the $c\bar{c}$ probability and will only increase that of the D^0D^{*0} component accordingly. Also note that the $c\bar{c}$ probability includes all ${}^3P_1$ states, with the $2\,{}^3P_1$ being dominant, because the corresponding bare eigenstate lies only 100 MeV higher. However, also the $1\,{}^3P_1$ state is non-negligible in the physical $X(3872)$ wave function. In the coupled-channel approach of Ref. [28], a $1\,{}^3P_1$ admixture of about 15% was found. Notice that — inevitably — unquenching not only mixes meson-meson components into the total bound-state wave function, but also quark-antiquark components of confinement states other than the one under consideration (also see Ref. [20]). Here, for a BE of 0.16 MeV, corresponding to the physical [6] $X(3872)$, case **X** in Table V, has a 7.48% $c\bar{c}$ probability for $a = 2.0$ GeV^{-1} and 11.18% for $a = 3.0$ GeV^{-1}. For smaller BEs, the $c\bar{c}$ probability decreases as expected, because of the growing weight of the D^0D^{*0} tail. On the other hand, for a BE of 10 MeV and $a = 3.0$ GeV^{-1}, the charmonium probability becomes even larger than that of the meson-meson component. Now, the experimental errors in the average mass of the $X(3872)$ and the D^0D^{*0} threshold allows for a maximum BE of 0.57 MeV, i.e., somewhere in between cases **X** and C. This would then correspond to a $c\bar{c}$ probability roughly midway in the range 7.48%–16.98% ($a = 2.0$ GeV^{-1}) or 11.18%–24.65% ($a = 3.0$ GeV^{-1}). In the limiting case of zero binding, the $c\bar{c}$ probability would eventually vanish. Also notice that, in all five cases of Table V, the $c\bar{c}$ probability rises by about 50% when a is increased from 2.0 to 3.0 GeV^{-1}. Nevertheless, if we take $a = 2.0$ GeV^{-1} as in our Ref. [14], we get a $c\bar{c}$ probability of 7.48%, very close the 7% found in Refs. [29, 30].

Next we use the normalized wave functions and Eq. (A11) to compute the $X(3872)$ r.m.s. radius for the five cases discussed before (see Table IV), with the results presented in Table VI. It is interesting to observe that the r.m.s. radius, which in principle is an observable, is much less sensitive to the choice of a than de wave-function probabilities. Furthermore, the large to very large r.m.s.

TABLE VI: R.m.s. radii of the wave function, expressed in fm, for the cases specified in Table IV.

a (GeV^{-1})	a (fm)	A	B	**X**	C	D
2.0	0.39	100.22	9.92	**7.82**	3.10	1.15
3.0	0.59	100.14	9.85	**7.76**	3.05	1.23

radii in the various situations are hardly surprising, in view of the small binding energies and the resulting very long tails of the D^0D^{*0} wave-function components (see Fig. 2 above).

Using Eq. (A12), we now also evaluate the S-wave scattering length $a_S = -\lim_{E\to 0}\left[k(E)\cot\delta_0(E)\right]^{-1}$. In case **X** and for $a = 2.0$ GeV^{-1} we thus find $a_s = 11.55$ fm, which is large yet of the expected order of magnitude for a BE of 0.16 MeV. For even smaller BEs, the scattering length will further increase, roughly like $\propto 1/\sqrt{\text{BE}}$. Let us here quote from Ref. [17]:

> *"Low-energy universality implies that as the scattering length a increases, the probabilities for states other than $D^0\bar{D}^{*0}$ or $\bar{D}^0D^{*0}$ decrease as $1/a$ ..."*

Indeed, we verify from our Table V that — very roughly — the $c\bar{c}$ probability decreases as $\propto \sqrt{\text{BE}}$, and so like $\propto 1/a_S$.

VI. STABILITY OF RESULTS AND NATURE OF POLES

In this section we are going to study the stability of our results, as well as the nature of the found solutions. So let us vary the two usually fixed parameters, viz. ω and m_c, in such a way that the bare $1\,^3P_1$ mass remains unaltered at 3599 MeV, whereas that of the $2\,^3P_1$ changes as shown in Table. VII. Thus, in case I E_1 is lowered by 25 MeV, while in case II it rises by 100 MeV. The trajectories for these two new situations are plotted in Fig. 3. For I we observe that, just as in the standard case depicted in Fig. 1, two poles are found relatively close to the real axis, of a dynamical and a confinement origin, respectively. However, now it is the $2\,^3P_1$ confinement pole that moves steadily downwards and settles on the real axis below threshold, whereas the dynamical pole moves to higher energies and eventually approaches the real axis. So the poles interchange their roles when going from the standard case to case I. Nevertheless, the values of g needed to get a bound state at 3871.68 MeV are not very different in the two cases, viz. 1.172 vs. 1.034. Such a behavior was already observed almost a decade ago, namely for the $D^*_{s0}(2317)$ [6] charmed-strange meson. In a first, two-channel model calculation [27] the $D^*_{s0}(2317)$ showed up as a dynamical resonance, settling below the S-wave DK threshold, whereas the $1\,^3P_0$ $c\bar{s}$ state turned out to move to higher energies, with a large width, similarly to the standard $X(3872)$ case in Figs. 1 and 3 above. However, in a more complete, multichannel approach [31] the situations got reversed, just as in the present case I. Also in our previous study [14] of the $X(3872)$, with nine

TABLE VII: Probability of $c\bar{c}$ component and $X(3872)$ r.m.s. radius for varying ω, m_c, with bare E_0 fixed at 3599 MeV, $X(3872)$ pole at 3871.68 MeV, and $a = 2.0$ GeV^{-1}.

	I	standard	II
E_1 (MeV)	3954	3979	4079
m_c (MeV)	1577.63	1562	1499.5
ω (MeV)	177.5	190	240
g	1.034	1.172	1.572
$c\bar{c}$ (%)	9.49	**7.48**	6.51
$r_{\text{r.m.s.}}$ (fm)	7.72	7.82	8.83

FIG. 3: Trajectories of dynamical and confinement poles. The bold curves represent cases I (top graph) and II (bottom graph) defined in Table VII, and the others the standard case of Fig. 1; the solid (dashed) lines stand for normal (below-threshold) resonances. All trajectories lie on the second Riemann sheet. The pole positions for the g values in Table VII are marked by $*$.

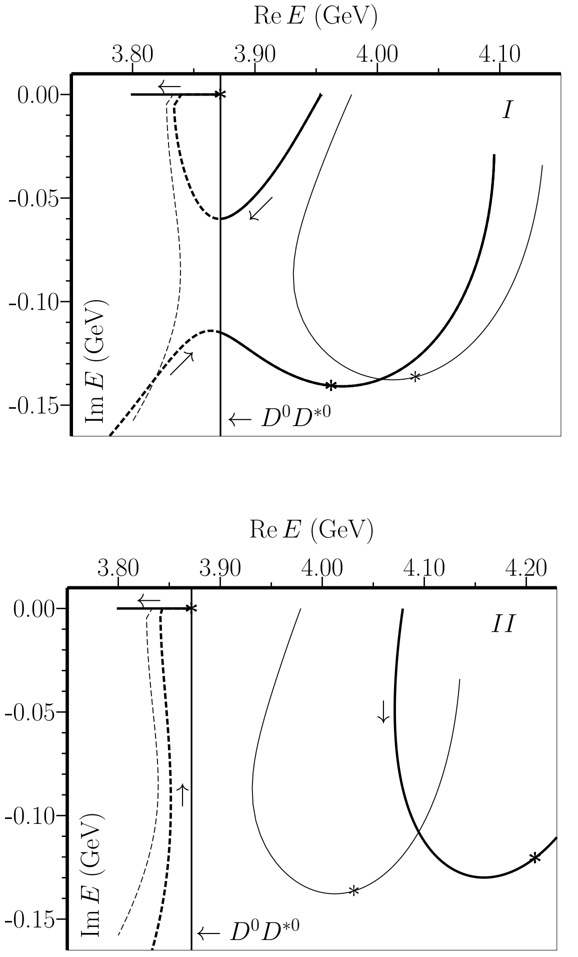

coupled channels, we reproduced the meson as a confinement pole. What appears to happen in the present case *I* is that shifting the bare $2\,^3P_1$ state to somewhat lower energies is just enough to make the confinement pole being deflected to the left and not the right when approaching the continuum pole. Clearly, there will be an intermediate situation for which the left/right deflection will hinge upon only marginal changes in the parameters, but resulting in two completly different trajectories. Therefore, identifying one pole as dynamical and the other as linked to a confinement state is entirely arbitrary, the whole system being dynamical because of unquenching. At the end of the day, the only thing that really counts is where the poles end up for the final parameters. The trajectories themselves are not observable and only serve as an illustration how a coupled-channel model as the one empoyed here mimics the physical situation. Suffice it to say that the lower pole, representing the $X(3872)$, is quite stable with respect to variations in the parameters, owing to its proximity to the only and most relevant OZI-allowed decay channel. The higher pole, on the other hand, should not be taken at face value, since a more realistic calculation should include other important decay channels, such as D^*D^*, with threshold just above 4 GeV.

Concerning the other scenario with changed parameters, labeled *II* in Table VII and depicted in the lower graph of Fig. 3, we see that the trajectories do not change qualitatively when going from the standard case to *II*. There is a displacement of the right-hand branch, about 100 MeV to the right on average, in accordance with the same shift of the bare $2\,^3P_1$ state. But the change in the lower, dynamical branch, is much less significant, though the value of g needed to produce a bound state at 3871-68 MeV now increases to 1.572 (see Table VII). We also notice from Fig. 3 that the two pole-trajectory branches hardly move towards one another, signaling less attraction between the poles due to a larger initial separation.

Inspecting again Table VII as for the $c\bar{c}$ probability in cases *I* and *II* compared to the standard situation, we observe an increased value for case *I* and a decreased one for *II*. This is logical, since in case *I* the bare $2\,^3P_1$ state lies closer to the $X(3872)$, whereas in case *II* it lies farther away. Nevertheless, the difference in $c\bar{c}$ probability between *I* and *II* is only about 3%, i.e., less than the variation with a in the standard case. These comparisons lend further support to the stability of our results.

Finally, in Fig. 4 we compare the wave function for case *II* with the standard one. We see there is no visible change in the R_f component. As for R_c, the first maximum gets somewhat reduced, but the secondary, negative bump even becomes a bit larger, owing to an inward shift of the node, lying now at about 3 GeV^{-1}. Yet, also in the case *II* the $c\bar{c}$ component is still very significant, despite the large separation of more than 200 MeV between the $X(3872)$ bound state and the bare $2\,^3P_1$ state.

From the latter and all previous results we may safely conclude that the $c\bar{c}$ component of the $X(3872)$ wave function remains nonnegligible in a variety of scenarios, being even of comparable size as the D^0D^{*0} component in the inner region, save at very short distances.

FIG. 4: Normalized two-component radial wave function $R(r)$, for cases *II* and "standard", corresponding to parameters in Table VII. Bold curves refer to case *II*, normal curve to R_c for standard case. Note: R_f is indistinguishable within graphical accuracy for the two cases.

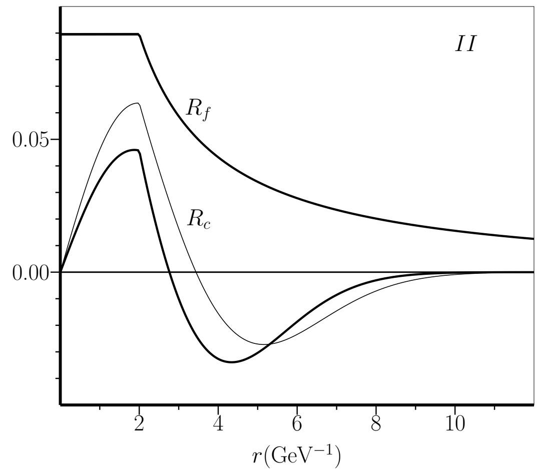

VII. SUMMARY AND CONCLUSIONS

In the present paper, we have employed a simple and solvable Schrödinger model to study the wave function of the $X(3872)$ meson, by treating it as a coupled $c\bar{c}$-D^0D^{*0} system with $J^{PC} = 1^{++}$ quantum numbers. Transitions between the two channels are described with the $^3P_0$ mechanism, through string breaking at a sharp distance a. The exact solutions to the equations allow us to easily study the trajectories of $\mathcal{S}$-matrix poles as a function of the decay coupling constant g. Thus, a dynamical pole is found, becoming a bound state just below the D^0D^{*0} threshold, for different string-breaking distances a, and an appropriate coupling g. On the other hand, the pole arising from the bare $2\,^3P_1$ confinement state moves to higher energies and aquires a large imaginary part. However, the latter pole may not be very relevant physically, because of neglected additional meson-meson channels that will become important in that energy region.

As for the $X(3872)$ radial wave function, the $c\bar{c}$ component R_c turns out to be of significant size as compared to the D^0D^{*0} component R_f, especially for intermediate r values. Moreover, even for other trial BEs, the global shape of R_c and its relative magnitude vis-à-vis R_f in the central region is remarkably stable. But the corresponding $c\bar{c}$ probability is relatively low, due to the very long tail of the D^0D^{*0} wave function at small binding. Quantitatively, for the average [6] $X(3872)$ binding of 0.16 MeV, a $c\bar{c}$ probability of 7.5–11.2% is found, for a in the range 0.4–0.6 fm, which is compatible with other recent approaches [29, 30]. The corresponding r.m.s. radius turns out to be quite stable at about 7.8 fm, for the latter range of a values, while the S-wave scattering length of 11.6 fm, for $a \approx 0.4$ fm, is in agreement with expectations for a BE of 0.16 MeV.

Finally, we have studied the nature of the $\mathcal{S}$-matrix pole giving rise to $X(3872)$, by varying some of the otherwise fixed parameters. Thus, a drastic modification of pole trajectories is observed, for relatively small parameter variations, making the $X(3872)$ pole transform from a dynamical pole into one directly connected to the $2\,{}^3P_1$ bare confinement state. However, the corresponding changes in the $c\bar{c}$ probability and r.m.s. radius, as well as the coupling g needed to reproduce $X(3872)$, are quite modest.

In conclusion, we should revisit the claims about $X(3872)$ made in Ref. [16], quoted in the Introduction above, namely about the inevitability of $X(3872)$ being a charm-meson molecule or virtual state, independently of the mechanism generating the state. Now, it is true that our analysis has confirmed some of the quantitative predictions in Ref. [16], viz. concerning the vanishing probability of wave-function components other than D^0D^{*0} as the BE approaches zero, and the related behavior of the D^0D^{*0} scattering length. However, we have also shown that the $c\bar{c}$ component is certainly not negligible and quite stable, in a variety of scenarios. Especially in electromagnetic processes, the prominence of this component for relatively small as well as intermediate r values will no doubt result in a significant contribution to the amplitudes. Moreover, as already mentioned above, the very unquenching of a $2\,{}^3P_1$ $c\bar{c}$ state will not only introduce meson-meson components into the wave function, but also a contribution of the $1\,{}^3P_1$ $c\bar{c}$ state, which can change predictions of electromagnetic transition rates very considerably [28]. We intend to study such processes for $X(3872)$ in future work, on the basis of a model as the one used in the present paper, by employing the formalism developed and successfully applied in Ref. [32].

For all these reasons, we do not consider $X(3872)$ a charm-meson molecule, but rather a very strongly unitarized charmonium state. As a matter of fact, we do not believe *any* non-exotic mesonic resonance — whatever its origin — qualifies as a true meson-meson molecule, simply because such a state will inexorably mix with the nearest $q\bar{q}$ states having the same quantum numbers. Indeed, we have demonstrated above that, even with a bare $c\bar{c}$ state 200 MeV higher in mass, the resulting $c\bar{c}$ component in the wave function is still appreciable. So let us conclude this discussion by quoting and fully endorsing the following statement from Ref. [16]:

> *"Any model of the* $X(3872)$ *that does not take into account its strong coupling to charm meson scattering states should not be taken seriously."*

Acknowledgments

One of us (G.R.) is indebted to R. M. Woloshyn for the invitation to a most stimulating miniworkshop at TRIUMF last year, where the topic leading to the present paper was debated. Thanks are also due to E. Braaten and K. K. Seth for very useful discussions on $X(3872)$. This work was partially supported by the *Fundação para a Ciência e a Tecnologia* of the *Ministério da Educação e Ciência* of Portugal, under contract no. CERN/FP/123576/2011.

Appendix A: Solving the coupled-channel Schrödinger equation

We twice integrate the Schrödinger equation (5) in order to get two sets of boundary conditions, viz. Eqs. (A1) and (A2):

$$\begin{aligned} u'_c(r\uparrow a) - u'_c(r\downarrow a) + \frac{g}{a}u_f(a) = 0\ , \\ u'_f(r\uparrow a) - u'_f(r\downarrow a) + \frac{g\mu_f}{a\mu_c}u_c(a) = 0\ ; \end{aligned} \tag{A1}$$

$$\begin{aligned} u_c(r\uparrow a) = u_c(r\downarrow a)\ , \\ u_f(r\uparrow a) = u_f(r\downarrow a)\ . \end{aligned} \tag{A2}$$

A general solution to this problem is the two-component wave function given by Eqs. (A3) and (A4), for the confined and meson-meson channel, respectively:

$$u_c(r) = \begin{cases} A_cF_c(r) & r < a\ , \\ B_cG_c(r) & r > a\ ; \end{cases} \tag{A3}$$

$$u_f(r) = \begin{cases} A_f J_{l_f}(kr)\ , & r < a\ , \\ B_f\Big[J_{l_f}(kr)k^{2l_f+1} & \\ \qquad \cot\big(\delta_{l_f}(E)\big) - N_{l_f}(kr)\Big]\ , & r > a\ . \end{cases} \tag{A4}$$

In Eq. (A3), the function $F_c(r)$ vanishes at the origin, whereas $G_c(r)$ falls off exponentially for $r \to \infty$, their explicit expressions being

$$F(r) = \frac{1}{\Gamma(l+3/2)}z^{(l+1)/2}e^{-z/2}\Phi(-\nu, l+3/2, z)\ , \tag{A5}$$

$$G(r) = -\frac{1}{2}\Gamma(-\nu)rz^{l/2}e^{-z/2}\Psi(-\nu, l+3/2, z)\ , \tag{A6}$$

where Φ and Ψ are the confluent hypergeometric functions of first and second kind (see Appendix B), respectively, $\Gamma(-\nu)$ is the complex gamma function, ν is given by Eq. (6), and $z = \mu\omega r^2$. Note that only in the case of integer ν, i.e., for $g = 0$, do Φ and Ψ reduce to the usual Laguerre polynomials for the three-dimensional HO potential. Furthermore, the functions J and N in Eq. (A4) are simple redefinitions of the standard spherical Bessel and Neumann functions, i.e., $J_l(kr) = k^{-l} r j_l(kr)$ and $N_l(kr) = k^{l+1} r n_l(kr)$. From the boundary conditions (A1) and (A2), as well as the wave-function expressions (A3) and (A4), we get, with the definition $\kappa = ka$,

$$G'_c(r)F_c(a) - F'_c(a)G_c(a) \;=\; \frac{g}{a} J_{l_f}(\kappa) F_c(a) \frac{A_f}{B_c} \;, \tag{A7}$$

$$J'_{l_f}(\kappa)N_{l_f}(\kappa) - J_{l_f}(\kappa)N'_{l_f}(\kappa) \;=\; \frac{g}{a}\frac{\mu_f}{\mu_c} J_{l_f}(\kappa) F_c(a) \frac{A_c}{B_f} \;.$$

Using now the Wronskian relations

$$W(F_c(a), G_c(a)) \equiv F_c(a)G'_c(a) - F'_c(a)G_c(a) = 1 \;, \tag{A8}$$

$$W(N_{l_f}(\kappa), J_{l_f}(\kappa)) \equiv N_{l_f}(\kappa)J'_{l_f}(\kappa) - N'_{l_f}(\kappa)J_{l_f}(\kappa) = -1 \;,$$

and continuity of the wave function at $r = a$ (cf. Eq. (A2)), we can solve for three of the four unknowns A_c, B_c, A_f, and B_f. Note that Eqs. (A1) and (A2) are not entirely linearly independent, so that solving all four constants is not possible. This is logical, as the overall wave-function normalization does not follow from the Schrödinger equation. Expressing all in terms of A_c then yields

$$A_c \;, \qquad A_f = -\left[\frac{g}{a} J_{l_f}(\kappa) G_c(a)\right]^{-1} A_c \;, \tag{A9}$$

$$B_c = \frac{F_c(a)}{G_c(a)}\, A_c \;, \qquad B_f = \frac{g}{a}\frac{\mu_f}{\mu_c} J_{l_f}(\kappa) F_c(a)\, A_c \;.$$

Note that, in order to obtain the $D^0 D^{*0}$ wave function in the outer region, we must substitute $\cot\left(\delta_{l_f}(E)\right) = i$ in Eq. (A4) (also see below). Finally, the normalization constant $\mathcal{N}$ of the total wave function is determined by computing

$$\int_0^\infty dr\ |u(r)|^2 = \int_0^\infty dr\ \left(u_c^2(r) + u_f^2(r)\right) = \mathcal{N}^2 \;. \tag{A10}$$

Then, we can also calculate the root-mean-square radius $\bar{r} = \sqrt{\langle r^2 \rangle}$ of the two-component system by

$$\langle r^2 \rangle = \frac{1}{\mathcal{N}^2} \int_0^\infty dr\, r^2 \left(u_c^2(r) + u_f^2(r)\right) \;. \tag{A11}$$

As for the $\mathcal{S}$-matrix poles corresponding to resonances, bound states, or virtual bound states, $\cot\left(\delta_{l_f}(E)\right)$ can be solved from continuity of $u_f(r)$ at $r = a$ in Eq. (A4), resulting in the expression

$$\cot\left(\delta_{l_f}(E)\right) = -\left[g^2 \frac{\mu_f}{\mu_c} k j_{l_f}^2(\kappa) F_c(a) G_c(a)\right]^{-1} + \frac{n_{l_f}(\kappa)}{j_{l_f}(\kappa)} \;, \tag{A12}$$

with the 1×1 $\mathcal{S}$ matrix simply given by

$$S_{l_f}(E) = \frac{\cot\left(\delta_{l_f}(E)\right) + i}{\cot\left(\delta_{l_f}(E)\right) - i} \;. \tag{A13}$$

Real or complex poles can then be searched for numerically, by using Newton's method to find the energies for which $\cot\left(\delta_{l_f}(E)\right) = i$, on the appropriate Riemann sheet.

Appendix B: Special functions, numerical methods, and kinematics

The confluent hypergeometric functions Φ and Ψ introduced in Appendix A are defined in Ref. [33], Eqs. (6.1.1) and (6.5.7), respectively. Thus, the function Φ is easily programmed as a rapidly converging power series, while the definition (6.5.7) of Ψ in terms of Φ and the gamma function Γ then also allows straightforward computation, by employing Gauss's multiplication formula for $\Gamma(-\nu)$ (see Ref. [34], Eq. (6.1.20)) so as to map the argument $-\nu$ to lying well inside the unit circle in the complex plane, whereafter a very fast converging power-series expansion of $1/\Gamma(-\nu)$ (see Ref. [34], Eq. (6.1.34)) can be applied.

The integrals for wave-function normalization and computation of r.m.s. radii are carried out by simple Gauss integration, choosing increasing numbers of points on a finite interval for the $c\bar{c}$ channel, and an infinite one for $D^0 D^{*0}$. Note that, in the former case, the wave function falls off fast enough to allow convergence for a finite cutoff, whereas in the latter a suitable logarithmic mapping is used. In both cases though, because of the wave-function cusp at $r = a$ and in order to avoid numerical instabilities, the domain of integration is split into two pieces, with up to 16 Gauss points in the inner region and 64 in the outer one, thus resulting in a very high precision of the results.

Although the $X(3872)$ bound state can reasonably be considered a nonrelativistic system, we still use relativistic kinematics in the $D^0 D^{*0}$ channel, since parts of the resonance-pole trajectories involve relatively large (complex) momenta. For consistency, the same is done for all energies. The manifest unitarity of the $\mathcal{S}$ matrix is not affected by this choice. Thus, the relative $D^0 D^{*0}$ momentum reads

$$k(E) = \frac{E}{2} \left\{ \left[1 - \left(\frac{T}{E}\right)^2\right] \left[1 - \left(\frac{P}{E}\right)^2\right] \right\}^{\frac{1}{2}} \;, \tag{B1}$$

where T and P are the threshold ($m_{D^{*0}} + m_{D^0}$) and pseudothreshold ($m_{D^{*0}} - m_{D^0}$) energies, respectively. The corresponding relativistic reduced mass is defined as

$$\mu_f(E) \equiv \frac{1}{2}\frac{dk^2}{dE} = \frac{E}{4}\left[1 - \left(\frac{TP}{E^2}\right)^2\right] \;. \tag{B2}$$

Note that in the $c\bar{c}$ channel the reduced mass is defined in the usual way, i.e., $\mu_c = m_c/2$, owing to the inherently nonrelativistic nature of the HO potential and the ensuing wave function.

---

[1] S. K. Choi *et al.* [Belle Collaboration], Phys. Rev. Lett. **91**, 262001 (2003).

[2] D. Acosta *et al.* [CDF Collaboration], Phys. Rev. Lett. **93**, 072001 (2004).

[3] V. M. Abazov *et al.* [D0 Collaboration], Phys. Rev. Lett. **93**, 162002 (2004).

[4] B. Aubert *et al.* [BABAR Collaboration], Phys. Rev. D **71**, 071103 (2005); **73**, 011101 (2006).

[5] R. Aaij *et al.* [LHCb Collaboration], Eur. Phys. J. C **72**, 1972 (2012).

[6] J. Beringer *et al.* [Particle Data Group Collaboration], Phys. Rev. D **86**, 010001 (2012).

[7] A. Abulencia *et al.* [CDF Collaboration], Phys. Rev. Lett. **98**, 132002 (2007).

[8] V. Bhardwaj *et al.* [Belle Collaboration], Phys. Rev. Lett. **107**, 091803 (2011).

[9] P. del Amo Sanchez *et al.* [BABAR Collaboration], Phys. Rev. D **82**, 011101 (2010).

[10] Y. Fan, J. -Z. Li, C. Meng, and K. -T. Chao, Phys. Rev. D **85**, 034032 (2012).

[11] T. Wang, G. -L. Wang, Y. Jiang,a and W. -L. Ju, arXiv:1205.5725 [hep-ph].

[12] C. -Y. Cui, Y. -L. Liu, G. -B. Zhang, and M. -Q. Huang, Commun. Theor. Phys. **57**, 1033 (2012).

[13] N. A. Tornqvist, Phys. Lett. B **590**, 209 (2004); Z. Phys. C **61**, 525 (1994); Phys. Rev. Lett. **67**, 556 (1991).

[14] S. Coito, G. Rupp, and E. van Beveren, Eur. Phys. J. C **71**, 1762 (2011).

[15] K. K. Seth, Prog. Part. Nucl. Phys. **67**, 390 (2012).

[16] E. Braaten and M. Lu, Phys. Rev. D **76**, 094028 (2007).

[17] E. Braaten and M. Kusunoki, Phys. Rev. D **69**, 074005 (2004).

[18] E. van Beveren and G. Rupp, Annals Phys. **324**, 1620 (2009).

[19] E. van Beveren and G. Rupp, Int. J. Theor. Phys. Group Theor. Nonlin. Opt. **11**, 179 (2006).

[20] E. van Beveren, C. Dullemond, and T. A. Rijken, Z. Phys. C **19**, 275 (1983).

[21] S. Coito, G. Rupp, and E. van Beveren, Acta Phys. Polon. Supp. **5**, 1015 (2012).

[22] E. van Beveren, T. A. Rijken, K. Metzger, C. Dullemond, G. Rupp, and J. E. Ribeiro, Z. Phys. C **30**, 615 (1986).

[23] E. van Beveren, G. Rupp, T. A. Rijken, and C. Dullemond, Phys. Rev. D **27**, 1527 (1983).

[24] A. M. Badalian, V. D. Orlovsky, and Y. A. Simonov, arXiv:1210.4674 [hep-ph].

[25] E. van Beveren and G. Rupp, arXiv:0712.1771 [hep-ph].

[26] G. S. Bali *et al.* [SESAM Collaboration], Phys. Rev. D **71**, 114513 (2005).

[27] E. van Beveren and G. Rupp, Phys. Rev. Lett. **91**, 012003 (2003).

[28] A. M. Badalian, V. D. Orlovsky, Y. .A. Simonov, and B. L. G. Bakker, Phys. Rev. D **85**, 114002 (2012).

[29] P. G. Ortega, J. Segovia, D. R. Entem, and F. Fernandez, Phys. Rev. D **81**, 054023 (2010).

[30] M. Takizawa and S. Takeuchi, arXiv:1206.4877 [hep-ph].

[31] E. van Beveren and G. Rupp, Phys. Rev. Lett. **97**, 202001 (2006); Eur. Phys. J. A **31**, 468 (2007).

[32] A. G. M. Verschuren, C. Dullemond, and E. van Beveren, Phys. Rev. D **44**, 2803 (1991).

[33] Bateman Manuscript Project, *Higher Transcendental Functions,* edited by A. Erdelyi *et al.*, (McGraw-Hill, New York, 1953), Vol. 1, Chap. VI.

[34] M. Abramowitz and I. A. Stegun, editors, *Handbook of mathematical functions, with formulas, graphs, and mathematical tables,* (Dover, New York, 1970), ninth printing, Chap. 6.